Phys Chem Minerals (2006) 32: 733–746
DOI 10.1007/s00269-005-0051-0

ORIGINAL PAPER

J. Filip · M. Novák · A. Beran · R. Zbořil

Crystal chemistry and OH defect concentrations in spodumene from different granitic pegmatites

Received: 17 August 2005 / Accepted: 27 October 2005 / Published online: 10 December 2005

Abstract Thirty spodumene samples of distinct paragenetic types (primary magmatic, secondary after petalite and hydrothermal) from variety of granitic pegmatites were characterized by electron microprobe, polarized FTIR spectroscopy and Mössbauer spectroscopy. The FTIR spectra of OH (weak sharp pleochroic bands at 3,425, 3,410, 3,395 cm^{-1} and in the 3,500–3,470 spectral region) are strongly polarized with maximum absorption parallel to n_γ. The majority of OH dipoles are presumably generated by a partial replacement of O2 oxygen atoms with an orientation pointing above the Li vacancy site. The separation of the bands probably resulted from a replacement of the coordinating Al by Fe and Si by Al. Homogeneous spodumene mostly close to its ideal formula $LiAlSi_2O_6$ shows Fe (0.00–0.10 apfu as Fe^{3+}; $Fe^{3+} >> Fe^{2+}$) and Na (0.00–0.04 apfu) as the only minor cations and $Fe^{3+}Al_{-1}$ substitution up to 10 mol% of the $LiFe^{3+}Si_2O_6$ component. Hydrogen concentrations (from 0.1 up to < 5 ppm H_2O by weight) vary as a function of genetic type with the highest amounts in high-temperature magmatic spodumene. Differences among particular genetic types of spodumene are related to maximum solubility of OH in spodumene structure at given P–T conditions and at actual chemical composition of spodumene. OH defect concentrations in spodumene follow a trend, LT/LP pyroxenes containing lower hydrogen contents compared to HT/HP ones. The hydrogen contents in particular genetic types of spodumene and their decrease with decreasing T and P are consistent with petrologic models of the pegmatite (sub)types formations.

Keywords Spodumene · EMP · FTIR · OH defect · Granitic pegmatites

J. Filip (✉) · M. Novák
Institute of Geological Sciences, Masaryk University in Brno,
Kotlářská 2, 611 37 Brno, Czech Republic
E-mail: filip@sci.muni.cz
Tel.: +420-58-5634947
Fax: +420-58-5225737

R. Zbořil · J. Filip
Centre for Nanomaterial Research and Department of Physical Chemistry, Palacky University in Olomouc,
Svobody 26, 771 46 Olomouc, Czech Republic

A. Beran
Department for Mineralogy and Crystallography,
University of Vienna—Geocentre, Althanstrasse 14,
1090 Wien, Austria

Introduction

Intensive research in the past few decades established that many nominally anhydrous minerals (NAMs) contain various concentrations of structurally incorporated hydrogen, thus acting as storage sites of significant quantities of water in the Earth's mantle (Bell and Rossman 1992; Ingrin and Skogby 2000; Beran and Libowitzky 2003). Study on hydrogen traces has high geological importance also because OH defects control the physical and chemical properties of minerals, including stability fields in P–T–X diagrams, rate of weathering, mineral deformation and rheologic properties (Rossman 1996).

Pyroxenes commonly contain variable but usually high amounts of structurally incorporated hydrogen as OH groups (Skogby et al. 1990; Skogby 1999; Ingrin and Skogby 2000). The hydrogen contents in pyroxenes and other NAMs may vary depending on both geological and crystal chemical factors (Ingrin and Skogby 2000) and could reflect the solid–fluid interactions during and/or after mineral formation. In contrast to the petrologically important mantle pyroxenes (Beran 1999; Ingrin and Skogby 2000; Koch-Müller et al. 2004), there is a lack of systematic studies dealing with hydrogen contents in less common upper crust pyroxenes. Lithium-bearing pyroxene—spodumene (ideally $LiAlSi_2O_6$)—is a typical accessory to major mineral in complex granitic pegmatites of the rare element class. We focused on the significance of hydrogen in such pyroxene formed under relatively low P–T conditions of upper crust because of

its importance as rock-forming mineral in Li-bearing pegmatites and its use as a raw material in ceramic industry.

The principal aim of this paper is to characterize distinct genetic types of spodumene from granitic pegmatites using electron microprobe analysis (EMPA) and both polarized Fourier transform infrared (FTIR) and Mössbauer spectroscopy. FTIR spectroscopy on single crystals is currently the most sensitive, non-destructive tool for detecting trace amounts of hydrogen bonded to oxygen. The intensity of IR absorption bands provides quantitative information on the OH defect concentration. Information on the OH incorporation mode is obtained using polarized IR radiation. The pleochroic scheme allows imposing defined constraints on the orientation of the OH dipole within the structure (Beran and Libowitzky 2003; Libowitzky and Beran 2004).

Sample description

Spodumene is monoclinic ($a = 9.449$ Å, $b = 8.386$ Å, $c = 5.215$ Å, $\beta = 110.10°$, $V = 388.1$ Å^3; Clark et al. 1969) with the space group $C2/c$, although the space group $C2$ is likely due to weak extra reflections (Clark et al. 1969; Graham 1975). Three oxygen positions occur in the pyroxene single-chain structure: O1 is the apical oxygen, O2 the "zigzag" and O3 the "chain" oxygen. The cation positions include the M1 site, occupied by octahedrally coordinated Al located between the O1 apices of the opposing tetrahedra, and the M2 sites, occupied by octahedrally coordinated Li lying between tetrahedra bases. Both M sites form edge-sharing chains, which run parallel to the (SiO_4) chains. The chemical composition of spodumene is commonly close to the ideal formula $LiAlSi_2O_6$. According to the data given in literature, mostly based on wet chemical analyses (London and Burt 1982; Charoy et al. 1992; Deer et al. 1997), minor cations found in spodumene include Fe (up to 1.58 wt% Fe_2O_3), Mn (up to 0.32 wt% MnO), Ca (up to 0.45 wt% CaO) and Na (up to 1.68 wt% Na_2O). Reported analytical water contents of up to 0.81 wt% might be related to microscopic inclusions of hydrous minerals (Charoy et al. 1992; Deer et al. 1997).

Three basic genetic types of spodumene (A, B and C) distinct in morphology, mineral assemblages and especially in their origin were distinguished in granitic pegmatites (see Table 1), generally consistent with those defined by London and Burt (1982). Primary magmatic spodumene (A) is the most abundant and it occurs in several pegmatite subtypes (Černý 1991; Černý and Ercit 2005). Albite-spodumene pegmatites (A1) occur as relatively thin sheet-like bodies, which exhibit quasi-homogeneous internal structure. Lath-shaped spodumene associated with fine-grained albite and blocky K-feldspar is commonly oriented subnormal to the contact of the pegmatite dikes (Kunasz 1982; Göd 1989). Albite-spodumene pegmatites are quite abundant and their origin is closely related to the peak of metamorphism of their host rocks (high-grade gneisses). Pegmatites of the spodumene subtype (A2) commonly form large zoned bodies, where lath-shaped crystals of spodumene occur in massive quartz or feldspar-rich intermediate units (Walker et al. 1986; Mulja et al. 1995). These pegmatites commonly occur in Abukuma-type metamorphic rocks (HT/LP terrains; cf. Spear 1993). Complex pegmatites of petalite, elbaite and/or lepidolite subtype (A3) are related to the spodumene subtype pegmatites. They contain primary spodumene as an accessory to minor mineral. These pegmatites form zoned bodies, where spodumene occurs in massive pegmatite (London 1986a; Foord et al. 1986, 1991); locally, as in Utö, Sweden, they occur in an endocontact zone of the petalite pegmatite (Smeds and Černý 1989). Coarse- to fine-grained quasi-homogeneous spodumene-bearing aplite-pegmatite bodies (A4) represent a specific type described only recently, where spodumene forms subhedral crystals and spodumene–quartz intergrowths. Spodumene-bearing aplite-pegmatite bodies are closely related to petalite-bearing aplite-pegmatites (Doria et al. 1989; Charoy et al. 1992, 2001).

Secondary spodumene (B) is a product of isochemical, late solidus to subsolidus breakdown of primary petalite according to the reaction: petalite = spodumene + quartz, chiefly from petalite subtype pegmatites (Černý et al. 1981; Černý 1982a, b, 2004; Chakoumakos and Lumpkin 1990). Spodumene forms coarse- to fine-grained intergrowths with quartz in pseudomorphs after petalite.

Table 1 *P–T* conditions of formation of individual spodumene types

Type	*T* (°C)	*P* (kbar)	Definition of the types	References
A1	~600	> 4	Albite-spodumene pegmatites	Göd (1989), Makrygina et al. (1990)
A2	550–600	3–5	Pegmatites of spodumene subtype	Chakoumakos and Lumpkin (1990), Černý (1991)
A3	550–600	3–5	Pegmatites of petalite, elbaite and/or lepidolite subtype	Chakoumakos and Lumpkin (1990), Černý (1991)
A4	480–520	2.5–2.8	Aplite-pegmatite bodies	Doria et al. (1989), Charoy et al. (1992)
B	400–550	2–3.5	Spodumene after petalite	Chakoumakos and Lumpkin (1990), Černý (1991), London and Burt (1982), London (2004)
C	< 450	< 1.8–2.5	Spodumene from pockets	London (1986a, b, 2004)

A Magmatic, *B* secondary, *C* hydrothermal

Hydrothermal spodumene (C) occurs as perfectly developed to locally etched crystals in pockets chiefly from complex pegmatites of elbaite or lepidolite subtype (Kazmi et al. 1985; London 1986a; Foord et al. 1991). Prismatic crystals (pink, green, colorless) are commonly associated with albite, quartz, K-feldspar, colored elbaite, pink beryl, muscovite and/or lepidolite.

The system $LiAlSiO_4$–SiO_2, including the phases spodumene, petalite, eucryptite, β-spodumene and quartz, was experimentally studied by London and Burt (1982), London (1984) and Krivovichev (2004). The estimated P–T conditions for individual types of spodumene, summarized in Table 1, exhibit large variations but specific P–T conditions were only scarcely available for individual localities. In addition, the P–T conditions derived from fluid inclusions studies are frequently controversial to those derived from phase equilibria and/or experimental work (compare London 1986a, b, 2004 versus Taylor et al. 1979 or London 1986a, b, 2004; Černý 2004 versus Thomas et al. 1990). It must also be considered that locally elevated Fe contents of natural spodumene crystals shift the position of the petalite/spodumene transition to different P–T conditions.

Experimental

Sample preparation

Thirty well-characterized spodumene samples covering defined genetic types (Table 1) were selected for chemical analyses and FTIR spectroscopic studies (Table 2). Only spodumene of the A4 type was not available in crystals of the quality suitable for spectroscopic investigations. The selected spodumene samples vary from small fragments of large grains or crystals with a good cleavage (primary and secondary spodumenes) to well-developed essentially gem-quality crystals (hydrothermal spodumene). Impurity-free single-crystal samples were crystallographically oriented by morphology, optical properties and X-ray single-crystal diffraction.

Two sets of slabs were prepared. (1) Well-developed gem-quality spodumene samples of hydrothermal origin (samples Sp07, Sp08, Sp10, Sp29 and SpPak; Table 2) were cut with a low-speed diamond saw and doubly polished parallel to the (100) and (010) planes. Sections parallel to the cleavage plane (110) were also prepared from the same samples Sp29 and SpPak for comparison. (2) Due to the quality of spodumene samples chiefly of primary and secondary and in part of hydrothermal origin, only cleavage plates parallel to (110) or (100) were prepared for the large number of remaining samples (see Table 3).

Analytical techniques

EMPA data of the spodumene samples used for the FTIR spectroscopic study were obtained on a CAMECA SX100 instrument equipped with five wavelength-dispersive spectrometers with large high-sensitive detection crystals operating at 15 keV accelerating voltage, 10 nA sample current, 5 μm beam diameter and 20 and 10 s (main elements) and 40 and 20 s (trace elements) counting times on peaks and background, respectively. Presence of particular elements was initially checked from energy-dispersive spectra. The following standards were used (K_α X-ray lines): albite (Na), andradite (Ca, Fe), almandine (Si), rhodonite (Mn), hornblende (Ti), sanidine (K, Al), olivine (Mg) and chromite (Cr). The analytical data were corrected and converted to concentrations with an X-phi routine (Merlet 1994) and with matrix-correction for the high Li content. The detection limits are: 0.02 for Ti, Cr and Mg; 0.03 for Na, Ca, K and Al; 0.04 for Fe and Si and 0.05 for Mn (all in wt%). The Li contents in spodumene were calculated from stoichiometry, Li = 1−(Na + K + Ca).

Polarized FTIR absorption spectra in the OH stretching frequency region of spodumene samples were recorded from 4,000 to 2,000 cm^{-1} using a Perkin Elmer FTIR 1760X spectrometer equipped with a TGS detector. For small crystals an attached Perkin Elmer FTIR microscope with external, LN_2-cooled MCT detector

Table 2 List of the studied samples

Sample no.	Locality	Source	Type
Sp14	Brandrucken, Styria, Austria	MM B7797	A1
Sp16	Cat Lake, Manitoba, Canada	MM B7830	A1
Sp26	Wildbachgraben, Styria, Austria	MM a 41	A1
SpKor	Weinebene, Styria, Austria	JF	A1
Sp01	Bakino, Kazakhstan	MM B7957	A2
Sp03	Villatuxe, Galicia, Spain	MM B5804	A2
Sp04	Tin Mountain, SD, USA	MM B7831	A2
Sp05	Lacorne Township, Ontario, Canada	MM a 861	A2
Sp06	Yellowknife, NWT Canada	MM B7829	A2
Sp12	Paton Lake, WI, USA	MM B8580	A2
Sp13	Otov, Czech Republic	MM a 3928	A2
Sp17	Tot Lake, Ontario, Canada	MM B7825	A2
Sp25	Etta Mine, SD, USA	MM a 1501	A2
Sp15	Manjaka, Madagascar	MM B10256	A3
Sp20	Newry, ME, USA	MM a 1531	A3
Sp21	Newry, ME, USA	MM a 161	A3
Sp22	Branchville, CT, USA	MM a 2509	A3
Sp23	Utö, Sweden	MM B8829	A3
Sp02	Bikita, Zimbabwe	MM a 894	B
Sp11	Silverleaf, Manitoba, Canada	MM B7828	B
Sp18	Tanco, Manitoba, Canada	MM B7826	B
Sp28	Tanco, Manitoba, Canada	MN	B
Sp07	Alexander Co., NC, USA	MM a 2831	C
Sp08	Vandeberg, Pala, CA, USA	MM B7836	C
Sp10	San Diego, Pala, CA, USA	MM B 312	C
Sp19	Madagascar	MM a 3178	C
Sp24	Pala, CA, USA	MM B314	C
Sp27a	Afghanistan	MB	C
Sp27b	Afghanistan	MB	C
Sp29	Nuristan, Afghanistan	JF	C
SpPak	Pakistan	EL	C

MM Moravian Museum, Brno, Czech Republic + catalogue nos.; *JF* sample of J. Filip; *MN* sample of M. Novák; *MB* sample of M. Bohatý; *EL* sample of E. Libowitzky

Table 3 Color, experimental data and mean analytical H_2O contents calculated on the basis of Beer's law (standard deviations are given for multiple measurements)

Sample no.[a]	Color	Plane	t (cm)	ν_m (cm^{-1})	ε_i (l mol^{-1} H_2O cm^{-2})	H_2O content (wt ppm)
Sp14	Grey	(100)	0.08	3,414	83,554	1.40(25)
Sp16	Grey	(100)	0.03	3,419	82,401	0.89(28)
Sp26	Colorless	(100)	0.12	3,429	79,880	0.82
SpKor	Green	(110)	0.02	3,418	82,520	1.73(28)
Sp01	Pale pink/white	(110)	0.02	3,412	84,126	3.78(59)
Sp03	Grey	(110)	0.04	3,412	84,177	3.43(78)
Sp04	White/gray	(110)	0.01	3,415	83,293	1.21(24)
Sp05	Green	(110)	0.02	3,422	81,624	0.44(18)
Sp06	Pale green	(110)	0.01	3,416	83,212	1.09(29)
Sp12	Colorless	(110)	0.04	3,417	82,887	0.61(2)
Sp13	Grey	(100)	0.03	3,432	79,101	2.49
Sp17	Colorless	(110)	0.03	3,417	82,849	0.63
Sp25	Pale green	(110)	0.23	3,402	86,455	1.81(24)
Sp15	Colorless	(110)	0.06	3,419	82,266	0.35(6)
Sp20	White	(110)	0.03	3,419	82,462	0.41
Sp21	Pinkish	(110)	0.18	3,434	78,626	0.42(10)
Sp22	Pinkish	(110)	0.03	3,417	82,801	0.72(22)
Sp23	Green	(110)	0.06	3,419	82,376	1.26(24)
Sp02	Pale green/gray	(110)	0.02	3,421	81,812	0.53(11)
Sp11	Colorless	(110)	0.04	3,421	81,850	0.57(31)
Sp18	White	(100)	0.04	3,416	83,152	0.64(25)
Sp28	Colorless	(100)	0.06	3,417	82,765	0.49(22)
Sp07	Green (hiddenite)	(100)	0.23	3,418	82,709	0.40[b]
		(010)	0.24			
Sp08	Colorless	(100)	0.10	3,417	82,893	0.32[b]
		(010)	0.13			
Sp10	Pink (kunzite)	(100)	0.25	3,417	82,980	0.24[b]
		(010)	0.25			
Sp19	Colorless	(110)	0.26	3,438	77,635	0.25
Sp24	Pink (kunzite)	(110)	0.30	3,429	79,855	0.39
Sp27a	Colorless	(110)	0.95	3,426	80,755	0.21
Sp27b	Pink (kunzite)	(100)	0.38	3,434	78,675	0.29
Sp29	Colorless	(100)	1.57	3,422	81,675	0.37[c]
		(010)	2.06			0.37[b]
		(110)	1.68			0.39[d]
SpPak	Pink (kunzite)	(100)	0.36	3,416	83,149	0.19[c]
		(010)	0.34			0.13[b]
		(110)	0.26			0.13[d]
Mean values				3,420	82,080	0.91

t thickness of crystal plates; ν_m the area-weighted mean wavenumber of all OH bands; ε_i integrated molar absorption coefficient
[a]The same order of samples as in Table 2
[b]Hydrogen content calculated using both (100) and (010) planes
[c]Hydrogen content calculated using only (100) plane
[d]Hydrogen content calculated using only (110) plane

and circular sample aperture with 100 μm diameter was used. A gold wire grid-polarizer with an extinction ratio better than 100:1 at $<3{,}500$ cm^{-1} was provided for the measurement of polarized IR spectra. A total of 100 scans in air were performed for each sample and the respective background with a resolution of 4 cm^{-1}. Absorption figures in the crystal sections were obtained after rotation of the polarizer over the range of 180° by steps of 10°. Spectra were deconvoluted into single Voigt-shaped absorption bands using the program PeakFit v4.0 (SPSS Inc.). Each sample was initially characterized using unpolarized IR radiation.

The ^{57}Fe Mössbauer spectra of spodumene with the highest Fe contents (samples Sp02, Sp05 and Sp23; Table 2) were recorded at room temperature in transmission geometry and in a constant acceleration mode. The ^{57}Co(Rh) source and a 1,024 register multi-channel analyzer were used. With respect to the relatively low Fe content, each spectrum was collected for about 4 days. The spectrum analyses were processed using a least-squares procedure assuming Lorentzian line shapes constrained to line width of 0.35 mm (two doublets of Fe^{2+}; see Dollase and Gustafson 1982) and using the distribution of quadrupole splitting (doublets of Fe^{3+}). Isomer shift values were calibrated with respect to an α-Fe foil.

Quantitative OH determination

A quantitative determination of the OH defect concentrations in spodumene was established for each sample

from polarized FTIR spectra on the basis of Lambert–Beer's law (Beran et al. 1993) in the form:

$$c_{\mathrm{wt\%}}\ \mathrm{H_2O} = (A_{\mathrm{i,total}} \times 1.8)/(t\varepsilon_i D).$$

The integrated absorbance values A_i ($\mathrm{cm^{-1}}$) measured parallel to the extinction directions on (010) and (100) plates must be summed up to get the total integrated absorbance value $A_{\mathrm{i,total}}$ ($A_{\mathrm{i,total}} = A_\gamma + A_\alpha + A_\beta$; Libowitzky and Rossman 1996). The thickness of the slabs t (cm) was measured with a digital micrometer and reported as an average of 3–5 measurements (reproducibility of ±0.001 mm; Table 3); the density of spodumene D equals 3.18 g $\mathrm{cm^{-3}}$ (Deer et al. 1997). As for most pyroxenes, no mineral-specific calibration for OH in spodumene exists (Bell et al. 1995). Due to the extremely low hydrogen concentration in spodumene and the presence of fluid inclusions in most of the samples, independent absolute calibration methods (e.g., SIMS, P_2O_5 cell coulometry, gas extraction manometry, nuclear reaction analysis) could hardly be applied. Approximations such as proposed by Paterson (1982) attempt to provide a way to deal with the dependence of integrated molar absorption coefficients ε_i (l $\mathrm{mol^{-1}}$ $\mathrm{H_2O}$ $\mathrm{cm^{-2}}$) on OH band positions. Based on polarized measurements of minerals with stoichiometric water contents, Libowitzky and Rossman (1997) established a linear calibration curve, $\varepsilon_i = 246.6$ ($\nu_m = 3{,}753$) where ν_m ($\mathrm{cm^{-1}}$) is the area-weighted average wavenumber of the OH peaks position. This calibration was used for the present study. Detailed polarized measurements parallel to the three axes of the optical indicatrix were performed on samples Sp07, Sp08, Sp10, Sp29 and SpPak (Table 3).

Results

Chemical composition

The spodumene samples were commonly found to be homogeneous in the BSE images and their chemical composition is generally close to the ideal formula (Table 4). The T site is occupied by Si in the stoichiometric amount 1.984–2.007 apfu (atoms per formula unit). The M1 site is occupied by Al varying from 0.891 to 1.010 apfu; low Al is compensated by substitution of Fe (both Fe^{3+} and Fe^{2+} up to 0.103 apfu). Only trace amounts of Mn (up to 0.008 apfu), Mg (up to 0.005 apfu), Ti (up to 0.003 apfu) and Cr (up to 0.002 apfu) were found. The M2 site includes only Na (up to 0.043 apfu) and negligible amounts of Ca and K (both up to 0.001 apfu) disregarding the not analyzed but dominant Li. No other elements were detected in spodumene.

Mössbauer spectroscopy of selected spodumene samples shows that both Fe^{2+} and Fe^{3+} are present (Fe^{3+} = 90–94% of Fe_{tot}; Fig. 1) and the calculated Fe^{2+} content vary from 0.004 to 0.007 apfu. Both Fe^{2+} and Fe^{3+} doublets have hyperfine parameters characteristic for octahedrally coordinated Fe (Table 5). Based on Fe_{tot}–$Al^{[6]}$ correlation and Mössbauer parameters, most of Fe^{3+} and Fe^{2+} occupy the M1 site. The second Fe^{2+} doublet with slightly smaller quadrupole splitting indicates that only minor amounts of Fe^{2+} could enter the M2 site also (cf. Dollase and Gustafson 1982; De Grave and Eeckhout 2003).

The individual spodumene samples exhibit minor to negligible differences in the concentrations of Fe and Na (Table 4, Fig. 2). The Fe contents reveal significant variations in the primary spodumene (Type A); up to 0.103 apfu of Fe_{tot} was found in the spodumene sample Sp23 from an endocontact zone of the petalite pegmatite near Utö, Sweden (A3). Secondary spodumene (B) and hydrothermal spodumene (C) commonly contain very low amounts of Fe, up to 0.003 and 0.009 apfu, respectively. Exceptionally high Fe contents were found in the pale green secondary spodumene sample Sp02 from Bikita, Zimbabwe (0.052 apfu) and in emerald green crystals of hydrothermal spodumene Sp07 from vugs in pegmatite of Stony Point, Alexander Co., North Carolina, USA (up to 0.031 apfu). Spodumene generally exhibits low Na contents up to 0.014 apfu (Fig. 2). Relatively high Na content up to 0.043 apfu was found solely in primary spodumene from albite-spodumene

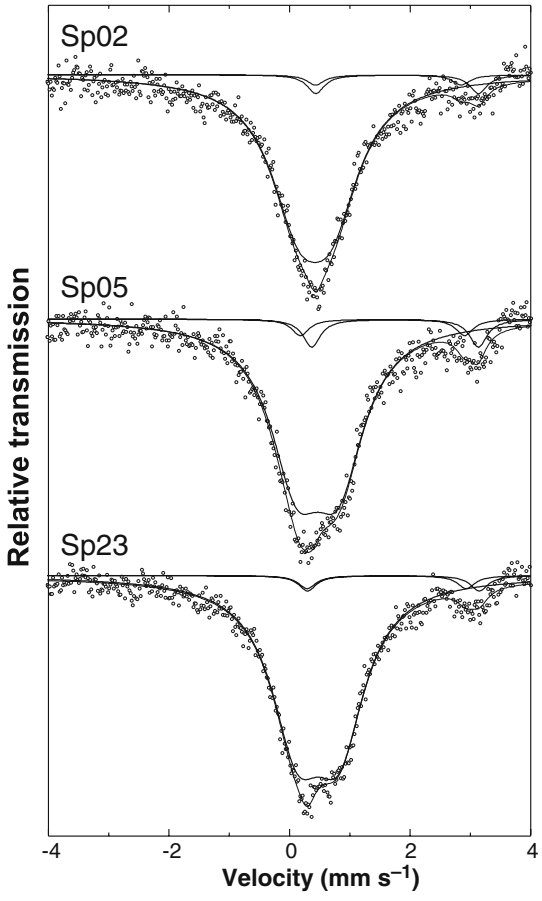

Fig. 1 Mössbauer spectra of spodumene samples with highest Fe contents

Table 4 Electron microprobe analyses and structural formulae of spodumene

Type		A1	A1	A1	A1	A2	A2	A2	A2	A2	A2	A2	A2	A2	A3
Sample no.		Sp14	Sp16	Sp26	SpKor	Sp01	Sp03	Sp04	Sp05	Sp06	Sp12	Sp13	Sp17	Sp25	Sp15
SiO_2		64.36	64.97	64.65	64.75	64.40	65.02	64.47	63.88	64.61	64.75	64.93	64.79	64.75	65.06
TiO_2		n.d.	n.d.	n.d.	n.d.	n.d.	n.d.	n.d.	n.d.	0.14	n.d.	n.d.	n.d.	0.06	n.d.
Al_2O_3		27.25	27.59	27.17	27.48	27.53	27.38	27.62	25.45	26.84	27.32	27.08	27.32	26.85	27.44
Fe_2O_3[b]		0.41	0.17	0.52	0.34	n.d.	0.23	0.20	3.23	1.41	0.27	0.59	0.16	0.98	0.15
CaO		n.d.	n.d.	n.d.	n.d.	0.04	n.d.	n.d.	0.03	n.d.	0.03	n.d.	n.d.	n.d.	n.d.
MgO		0.02	n.d.	n.d.	n.d.	n.d.	n.d.	n.d.	n.d.	n.d.	n.d.	n.d.	n.d.	0.04	n.d.
MnO		0.08	0.09	0.07	0.09	n.d.	0.09	0.09	0.29	0.07	0.12	n.d.	0.07	0.12	0.06
Li_2O[c]		7.68	7.88	7.70	7.41	7.70	7.67	7.73	7.50	7.74	7.85	7.54	7.80	7.98	7.90
Na_2O		0.39	0.09	0.71	0.34	0.13	0.16	0.15	0.15	0.14	0.13	0.21	0.08	0.16	0.15
K_2O		n.d.	n.d.	n.d.	n.d.	n.d.	n.d.	n.d.	0.03	0.03	n.d.	n.d.	0.03	n.d.	n.d.
Total		100.19	100.79	100.82	100.41	99.80	100.55	100.26	100.56	100.98	100.47	100.35	100.25	100.94	100.76
		Number of cations on the basis of 6 oxygens													
T	Si^{4+}	1.994	1.996	1.998	1.994	1.996	2.000	1.991	1.989	1.990	1.998	2.001	2.000	1.997	2.001
M1	Al^{3+}	0.995	0.999	0.989	0.998	1.005	0.993	1.005	0.934	0.974	0.994	0.984	0.994	0.976	0.995
	Fe^{3+}	0.010	0.004	0.012	0.008	–	0.005	0.005	0.076	0.033	0.006	0.014	0.004	0.023	0.003
	Mg^{2+}	0.001	–	–	–	–	–	–	–	–	–	–	–	0.002	–
	Mn^{2+}	0.002	0.002	0.002	0.002	–	0.002	0.002	0.008	0.002	0.003	–	0.002	0.003	0.002
	Ti^{4+}	–	–	–	–	–	–	–	–	0.003	–	–	–	0.001	–
∑ M1		1.008	1.005	1.003	1.008	1.005	1.000	1.012	1.018	1.012	1.003	0.998	1.000	1.005	1.000
M2	Li^{+}	0.977	0.995	0.957	0.980	0.991	0.990	0.991	0.989	0.991	0.991	0.987	0.994	0.990	0.991
	Na^{+}	0.023	0.005	0.043	0.020	0.008	0.010	0.009	0.009	0.008	0.008	0.013	0.005	0.010	0.009
	Ca^{2+}	–	–	–	–	0.001	–	–	0.001	–	0.001	–	–	–	–
	K^{+}	–	–	–	–	–	–	–	0.001	0.001	–	–	0.001	–	–
∑ Cat.		4.002	4.001	4.001	4.002	4.001	4.000	4.003	4.007	4.002	4.001	3.999	4.000	4.002	4.001

n.d. not detected (i.e., below the detection limit of EMPA)
[a]Sample Sp07 contains 0.07 wt% Cr_2O_3 (0.002 apfu Cr)
[b]All Fe as Fe_2O_3
[c]Calculated from stoichiometry

pegmatites (A1) except Na-poor spodumene from the locality Cat Lake, Manitoba (A1, Sp16) which is comparable to the other spodumene types (Table 4).

Polarized IR spectroscopy

The FTIR spectra of spodumene in the OH stretching frequency region consists of a series of weak and relatively sharp pleochroic OH absorption bands, located in the 3,350–3,550 cm^{-1} range (Fig. 3a–d). Two separate OH regions can be discerned. (1) Bands centered around 3,395, 3,410 and 3,424 cm^{-1} (half-widths ca. 10 cm^{-1}) represent a characteristic band triplet. Their mutual intensity ratios vary (Fig. 3a), but the band centered at 3,410 cm^{-1} is usually the strongest in all spodumene spectra. (2) Bands centered at around 3,474–3,490 cm^{-1} are of much lower intensities than the low-energy bands (Fig. 3a–d) and they are missing in some samples.

Except the band centered at 3,474 cm^{-1}, all OH bands are strongly pleochroic (Fig. 3c, d), with an average maximum/minimum ratio of about 7/1. The band triplet with maxima at 3,395, 3,410 and 3,424 cm^{-1} and the high-energy bands at around 3,490 cm^{-1} reveal an identical pleochroic behavior, showing maximum absorption in the (010) plane, when the vector **E** of the polarized radiation vibrates parallel to the n_γ direction of the indicatrix which inclines approximately 25° to the *c* axis (measured on samples Sp07, Sp08, Sp10, Sp29 and SpPak; Fig. 4). Consequently, minimum absorption occurs parallel to the n_α direction. In (100) plates these bands show maximum absorption when the **E** vector vibrates parallel to the *c* axis (parallel to n'_γ) and a weak absorption component parallel to the *b* axis, which corresponds to the direction of n_β (Fig. 4). The three-dimensional absorption figure corresponds to a lemniscate, rotating around the long axis (n_γ). Distinct pleochroism is evident for the band at 3,474 cm^{-1}, where a slightly stronger absorbance can be observed parallel to n_α in (010) plates and parallel to n_β in (100) plates (Figs. 3c, 4). Absorption figures measured on (110) cleavage plates of samples Sp01, Sp03, Sp27a, Sp24, Sp29 and SpPak are very similar to those measured on (010) (Fig. 4, bottom).

OH defect concentration

The mean ε_i value for spodumene calculated from the calibration of Libowitzky and Rossman (1997) amounts to 82,080 (1,600) l $mol^{-1}{}_{H2O}$ cm^{-2} and is very close to the ε_i value reported by Bell et al. (1995) for orthopyroxene [80,600 (3,200) l $mol^{-1}{}_{H2O}$ cm^{-2}], determined on the basis of a calibration by hydrogen manometry. This value is more than twice higher than that determined for

A3 Sp20	A3 Sp21	A3 Sp22	A3 Sp23	B Sp02	B Sp11	B Sp18	B Sp28	C Sp07[a]	C Sp08	C Sp10	C Sp19	C Sp24	C Sp27	C Sp29	C SpPak
65.53	65.13	65.17	63.76	64.32	65.06	64.74	64.99	65.21	65.19	65.20	65.16	65.01	65.10	65.14	64.26
n.d.	0.03	n.d.	n.d.	0.02	n.d.	0.03	n.d.	n.d.	n.d.	n.d.	n.d.	n.d.	n.d.	n.d.	n.d.
27.64	27.48	27.65	24.08	26.28	28.00	27.16	27.74	27.02	27.69	27.57	27.74	27.61	27.36	27.13	27.60
0.18	n.d.	0.18	4.37	2.25	n.d.	0.04	n.d.	1.33	n.d.	n.d.	n.d.	0.11	0.17	0.40	n.d.
n.d.	n.d.	n.d.	n.d.	n.d.	n.d.	n.d.	n.d.	0.03	0.03	n.d.	n.d.	n.d.	n.d.	n.d.	0.03
n.d.	n.d.	n.d.	n.d.	0.02	n.d.	n.d.	n.d.	0.10	n.d.	n.d.	n.d.	n.d.	n.d.	n.d.	n.d.
0.06	0.07	0.21	0.10	0.27	n.d.	0.05	n.d.	n.d.	0.07	0.08	n.d.	n.d.	0.08	0.10	0.10
7.82	7.97	8.02	7.76	7.80	7.74	7.94	8.06	7.29	7.55	7.48	8.01	8.04	8.03	7.55	7.59
0.12	0.13	0.13	0.15	0.14	0.11	0.06	0.06	0.19	0.14	0.14	0.10	0.10	0.11	0.15	0.23
n.d.	n.d.	n.d.	n.d.	n.d.	n.d.	n.d.	n.d.	n.d.	n.d.	n.d.	n.d.	n.d.	n.d.	0.03	n.d.
101.35	100.81	101.36	100.22	101.10	100.91	100.02	100.85	101.17	100.67	100.47	101.01	100.87	100.85	100.50	99.81
2.000	2.001	1.996	2.003	1.988	1.992	2.005	1.996	1.994	1.998	2.000	1.998	1.998	2.002	2.004	1.992
0.994	0.995	0.998	0.891	0.957	1.010	0.991	1.004	0.974	1.000	0.997	1.002	1.000	0.992	0.984	1.008
0.004	–	0.004	0.103	0.052	–	0.001	–	0.031	–	–	–	0.003	0.004	0.009	–
–	–	–	–	0.001	–	–	–	0.005	–	–	–	–	–	–	–
0.002	0.002	0.005	0.003	0.007	–	0.001	–	–	0.002	0.002	–	–	0.002	0.003	0.003
–	0.001	–	–	0.000	–	0.001	–	–	–	–	–	–	–	–	–
1.000	0.998	1.007	0.997	1.017	1.010	0.994	1.004	1.010	1.002	0.999	1.002	1.003	0.998	0.996	1.011
0.993	0.992	0.992	0.991	0.992	0.993	0.996	0.996	0.988	0.991	0.992	0.994	0.994	0.993	0.990	0.985
0.007	0.008	0.008	0.009	0.008	0.007	0.004	0.004	0.011	0.008	0.008	0.006	0.006	0.007	0.009	0.014
–	–	–	–	–	–	–	–	0.001	0.001	–	–	–	–	–	0.001
–	–	–	–	–	–	–	–	–	–	–	–	–	–	0.001	–
4.000	3.999	4.003	4.000	4.005	4.002	3.999	4.000	4.004	4.000	3.999	4.000	4.001	4.000	4.000	4.003

clinopyroxene [38,300 (1,700) l $mol^{-1}{}_{H2O}$ cm^{-2}; Bell et al. 1995]. As there are striking similarities in the spectral features of spodumene and orthopyroxenes, especially the presence of a dominating band at 3,410 cm^{-1} (Skogby et al. 1990; Stalder 2004), similarities in the absorption coefficients can be expected.

The monoclinic symmetry of spodumene renders absorbance measurements parallel to the three axes of the optical indicatrix ($A_{i,total} = A_\gamma + A_\alpha + A_\beta$) inconvenient. Based on the knowledge of the three-dimensional absorption figure from samples Sp07, Sp08, Sp10, Sp29 and SpPak (see previous section) showing comparable components parallel to n_α and n_β (Fig. 4), more convenient approaches are developed by simply measuring the absorbances parallel to the n'_γ and n'_α extinction directions on (110) cleavage planes or parallel to n'_γ and n_β on (100) planes. For samples where only (110) cleavage plates were measured, $A_{i,total} = A'_\gamma + 2A'_\alpha$ or alternatively for (100) plates, $A_{i,total} = A'_\gamma + 2A_\beta$.

The comparison of hydrogen contents calculated from absorbances measured parallel to the n_α, n_β and n_γ directions on (100) and (010) planes with contents calculated from absorbances measured parallel to the n'_γ and n'_α extinction directions on solely (110) and parallel to n'_γ and n_β on (100) plane is given for samples Sp29 and SpPak in Table 3. Due to the simplicity of preparing spodumene cleavage slabs and introducing a low error during such approach (cf. Table 3), this method is quite convenient. In ideal cases, unpolished cleavage plates can be used for the (semi)quantitative determination of the trace hydrogen content. In order to establish inhomogeneities of the OH distribution within one sample, multiple measurements of 2–6 grains from most of the samples were performed. Hence, Table 3 shows mean values of OH defect concentrations with respective standard deviations for multiple measurements.

The studied spodumene samples contain extremely low OH defect concentrations ranging from 0.13 to 3.78 wt ppm H_2O (mean values for respective samples; Table 3), whereas the maximum values for individual samples amount to 4.7 wt ppm H_2O (Fig. 5). However, Skogby et al. (1990) found apparently higher concentrations of 410 wt ppm OH (=205 wt ppm H_2O) for spodumene from Pala, Southern California, USA. Our study of hydrothermal spodumene from the same region (Sp08, Sp10 and Sp24) revealed 0.32, 0.24 and 0.38 wt ppm H_2O (Table 3) calculated according to the calibration of Libowitzky and Rossman (1996, 1997). Significant differences in total hydrogen contents are obvious partly because Skogby et al. (1990) used linear intensities (peak heights) instead of absorption areas to estimate the OH contents (see, e.g., Bell et al. 2004) and probably also due to misinterpreting absorption bands of water from fluid inclusions or bands corresponding to

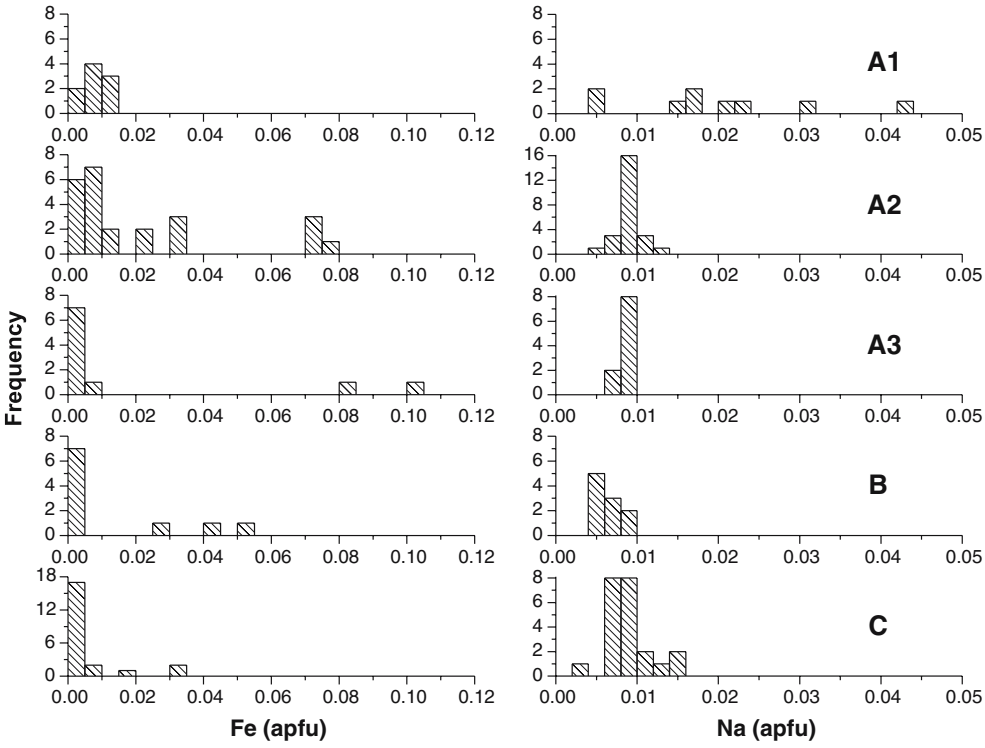

Fig. 2 Iron (*left*) and sodium (*right*) contents for spodumene samples of different genetic types. Note the different frequency scales for different spodumene types

inclusions of phyllosilicates or due to sample preparation (cf. Keppler and Rauch 2000). The hydrogen content calculated using band intensities to get A_i and using the same calibration as in Skogby et al. (1990) yielded 37.5, 30 and 39 wt ppm OH for the samples Sp08, Sp10 and Sp24, respectively. From our results on large number of spodumene samples (this study), the unusually high OH concentrations reported for a single spodumene sample (Skogby et al. 1990) seems to be overestimated (cf. Bell et al. 2004).

Apparent differences in the hydrogen contents of spodumene from various genetic types are evident (Table 3, Fig. 5). Magmatic spodumene displays the highest hydrogen contents; moderate variations occur in the A1 (0.82–1.73 wt ppm H_2O) and the A3 types (0.35–1.26 wt ppm H_2O), high variations in the A2 type (0.44–3.78 wt ppm H_2O). The highest H_2O contents were found in spodumene from Bakino, Kazakhstan (Sp01, up to 4.7 wt ppm, mean 3.78 wt ppm) and from Villatuxe, Galicia, Spain (Sp03, up to 4.1 wt ppm, mean 3.43 wt ppm). Secondary spodumene exhibits low hydrogen concentrations with values ranging from 0.49 to 0.64 wt ppm H_2O and hydrothermal spodumene reveals the lowest values, ranging from 0.13 to 0.40 wt ppm H_2O.

The FTIR spectra of a single crystal of a pink spodumene (kunzite, SpPak), thermally treated in a furnace in air at 300, 400, 800 and 900°C for 2 h, show no decrease of the OH band intensity up to 400°C and moderate decrease between 400 and 900°C, with decrease up to 60% of the initial value at the highest temperature. The band at 3,410 cm^{-1} is slightly more reduced than the other bands. Heating up to 300°C for 2 h reduced satisfactorily the background. At 300°C and particularly at 400°C, a loss of the pink color was observed.

Discussion

Crystal chemistry

The EMP study confirms that spodumene is mostly close to its ideal composition (see Table 4). Minor amounts of Fe ($Fe^{3+} >> Fe^{2+}$) and Na suggest the presence of aegirine ($NaFe^{3+}Si_2O_6$), jadeite ($NaAlSi_2O_6$) and/or Fe-

Table 5 Mössbauer parameters for selected spodumene samples

Sample no.	Subspectra	Hyperfine parameters		RA (%)
		δ (mm s^{-1})	ΔE_Q (mm s^{-1})	
Sp02	$^{[6]}Fe^{2+}$	1.79	2.70	4.6
	$^{[6]}Fe^{2+}$	1.64	2.42	2.5
	$^{[6]}Fe^{3+}$	0.42	0.55	92.9
Sp05	$^{[6]}Fe^{2+}$	1.74	2.76	6.1
	$^{[6]}Fe^{2+}$	1.53	2.72	3.5
	$^{[6]}Fe^{3+}$	0.45	0.70	90.4
Sp23	$^{[6]}Fe^{2+}$	1.72	2.85	3.4
	$^{[6]}Fe^{2+}$	1.61	2.64	2.8
	$^{[6]}Fe^{3+}$	0.48	0.70	93.8

δ isomer shift, ΔE_Q quadrupole splitting, *RA* relative spectrum area

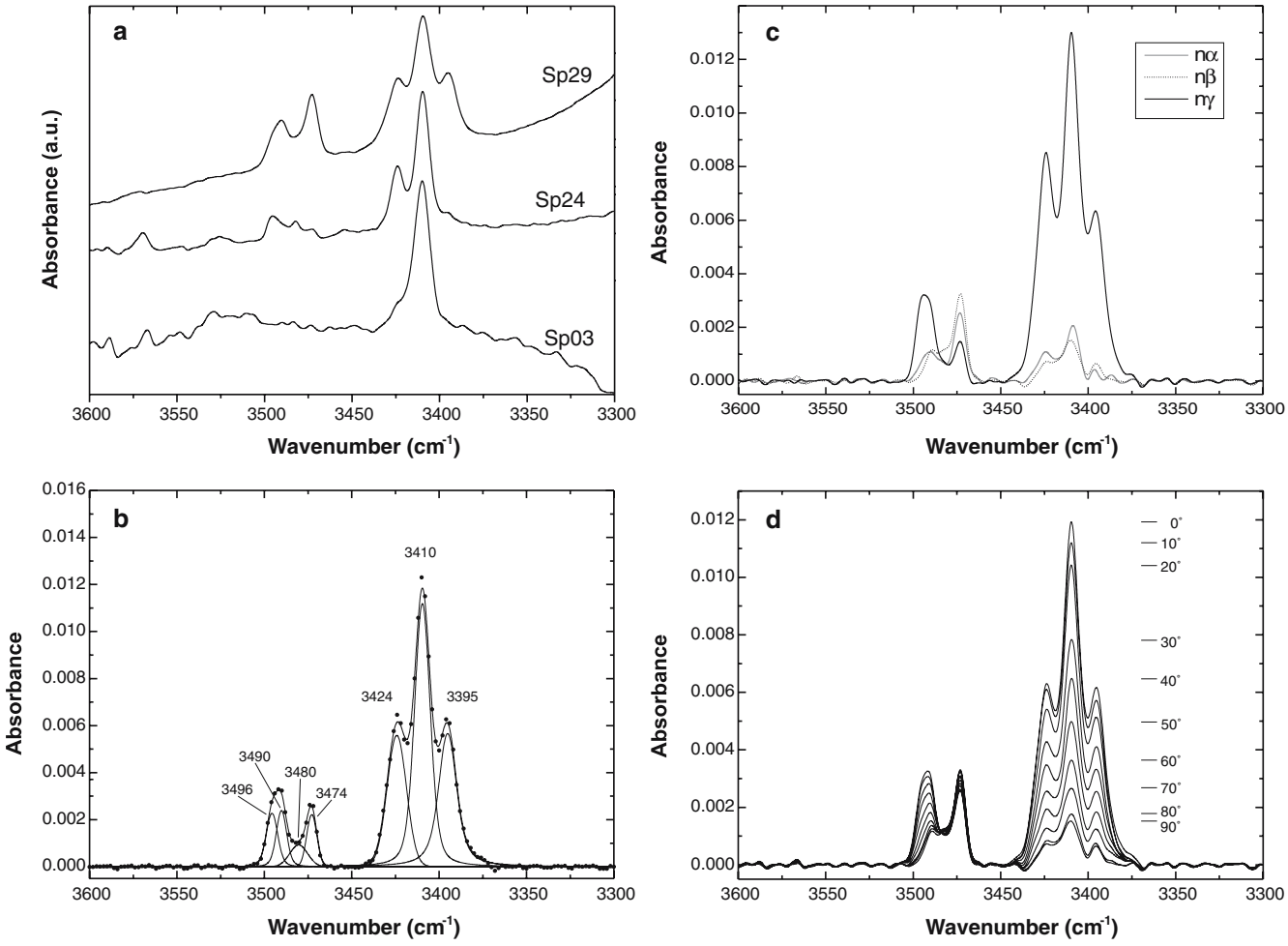

Fig. 3 **a** Representative OH absorption spectra (non-polarized IR radiation) of spodumene. Individual spectra are offset vertically for clarity and multiplied to fit the frame. **b** Polarized FTIR absorption spectrum of Sp29 approximately parallel to n_γ with fitted bands. **c** Polarized FTIR absorption spectra of Sp29 measured with **E** parallel to n_γ, n_α and n_β directions. **d** Polarized FTIR spectra measured from 0° to 90° within (100) plane of sample Sp29. **b**–**d** Spectra normalized to 1 mm of sample thickness

spodumene ($LiFe^{3+}Si_2O_6$) components (up to 10 mol%). From the negative correlation of Fe^{3+} and Al (cf. Table 4) it is evident that most of the Fe enters the M1 site. This observation is supported by wide Mössbauer doublets (Fig. 1) indicating, moreover, a random distribution of Fe on M1 sites, which may play an important role in the incorporation of hydrogen into the spodumene structure, forming only a limited number of preferable sites.

Whereas the Fe content in spodumene from Utö, Sweden (Sp23; A3) is the highest ever recorded, Na concentrations are distinctly lower than those given in the literature (London and Burt 1982; Charoy et al. 1992; Deer et al. 1997). The additional minor cations in spodumene include Mn (up to 0.29 wt% MnO—0.008 apfu), which is comparable, and Ca (up to 0.04 wt% CaO—0.001 apfu), which is much lower relative to the data given in the literature (London and Burt 1982; Charoy et al. 1992; Deer et al. 1997). Higher concentrations of Na and Ca given in the literature (see Sample description) very likely reflect the distinctly employed methods, EMP analysis (this work) versus wet chemical analysis (e.g., Charoy et al. 1992), because inclusions of feldspars and/or of phyllosilicates may increase concentrations of the particular elements determined by bulk chemical analyses.

Very low Fe content in secondary spodumene can be explained by low Fe in primary petalite, a spodumene precursor (London and Burt 1982). However, pale green spodumene from Bikita, Zimbabwe (Sp02), is the only Fe-enriched secondary spodumene after petalite known up to date. It is associated with quartz and secondary black tourmaline, and Fe enrichment in the spodumene–quartz–tourmaline aggregate from Bikita is not clear.

There are commonly low Na contents in spodumene; only spodumene from albite-spodumene pegmatites (A1) yielded elevated Na. These pegmatites very likely originated at high pressure relative to other spodumene pegmatites (Table 1), hence higher content of jadeite component may reflect higher pressures as in other geological environments (cf. Spear 1993).

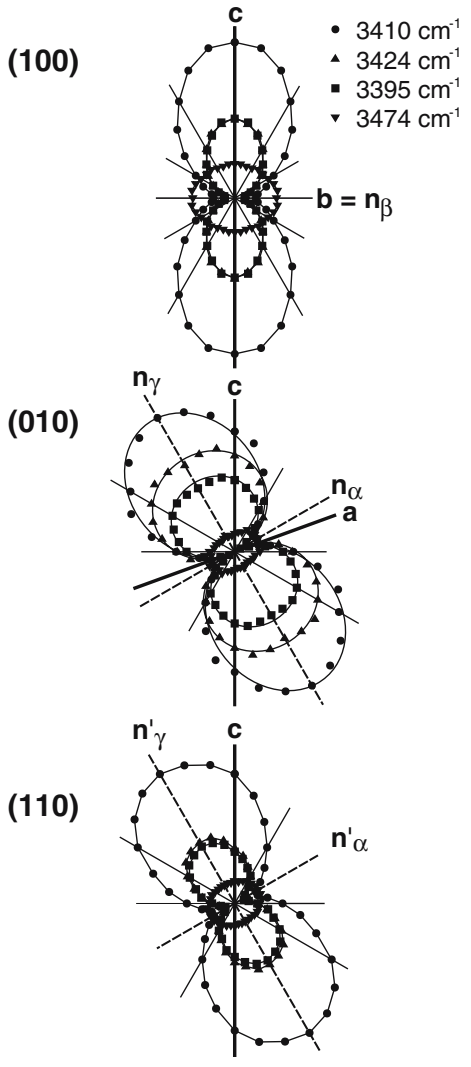

Fig. 4 Experimentally obtained angular absorbance figures for (100), (010) and (110) planes of sample Sp29. With respect to the strong overlap in the central parts, angular absorbance figures of the less intense 3,480, 3,490 and 3,496 cm^{-1} bands are not shown

Model of OH defect incorporation

Pleochroic behavior of sharp OH bands and results of heating experiments clearly show that hydrogen in spodumene is of point structural defect nature (cf. Rossman 1996; Koch-Müller et al. 2004). The prominent OH bands of spodumene centered at 3,395, 3,410 and 3,424 cm^{-1} are distinct from those of most natural clinopyroxenes where significantly broader OH absorption bands usually occur at higher wavenumbers. However, spodumene spectra are similar to those of orthopyroxenes showing prominent sharp bands at 3,410, 3,510 and 3,560 cm^{-1} (Skogby et al. 1990; Beran and Libowitzky 2003). Comparing the OH absorption spectra of amphiboles (3,700–3,600 cm^{-1}) and sheet silicates (3,750–3,550 cm^{-1}) (Farmer 1974; Skogby and Rossman 1989; Beran 2002), no absorption features related to these minerals are evident in the spectra of spodumene. Thus common alteration of pyroxenes to hydrous silicates (pyroxene + SiO_2 + H_2O = amphibole, Veblen and Buseck 1981; Skogby and Rossman 1989), leading to (sub)microscopic intergrowths of biopyribole lamellae, clearly does not occur in spodumene.

Two OH absorption band regions in the IR spectra of spodumene imply that there are two slightly different mechanisms for hydrogen incorporation into the spodumene structure. An additional OH defect type is indicated by the 3,474 cm^{-1} band with a different pleochroic behavior (Figs. 3, 4). Owing to the pleochroic scheme of the triplet band at 3,395, 3,410 and 3,424 cm^{-1} in (010), the OH dipole direction must be oriented roughly parallel to the n_γ. In addition, a slight deviation from the (010) plane is indicated in (100) by a weak component parallel to n_β. An OH dipole direction that is in agreement with the observed pleochroic behavior can be provided if vacancies in the M2 site are assumed. OH defects coordinated by one Al and one Si are generated by a partial replacement of O2 oxygen atoms with an orientation pointing towards the vacancy in the Li site (Fig. 6). The separation of the bands probably resulted from a replacement of the coordinating Al by Fe and Si by Al. The comparable pleochroism of the high-energy band around 3,490 cm^{-1} can be explained by OH dipoles partially replacing the O1 sites. Assuming vacant M1 site lying in the Si–O1–M1 plane, an OH group coordinated by one Si, one Al and one Li and pointing to a vacant Al site is deduced (Fig. 6). The pleochroic scheme of the low-energy band triplet and the single high-energy band is comparable to that of the weak low-energy band doublet in diopside (Beran and Libowitzky 2003; Libowitzky and Beran 2004). A slightly preferred orientation of an OH defect within the (001) plane is deduced from the weak pleochroism of the band at 3,474 cm^{-1}. According to similarities with OH dipole in the diopside structure (Beran and Libowitzky 2003), this absorption behavior is explained by a partial replacement of O2 by OH defects pointing to the O3 oxygen atom of a neighbored silicate (SiO_4) chain. Compared to diopside and other pyroxenes where most of OH dipoles lie parallel to n_α (Beran and Libowitzky 2003; Libowitzky and Beran 2004), the preferred orientation of OH dipoles in the spodumene structure is generally in an opposite trend (roughly parallel to the n_γ). Based on the mean stretching frequency of OH bands in spodumene ($\nu_m = 3{,}420$ cm^{-1}), O–H···O distances of about 2.8 Å are deduced from the distance–frequency correlation of Libowitzky (1999).

Factors controlling hydrogen incorporation

(1) External factors as geological setting during crystallization, including variable activity of hydrous component, oxygen fugacity or *P*–*T* conditions (Skogby and Rossman 1989; Bai and Kohlstedt 1993; Losos and Beran 2004), and (2) internal factors as crystal

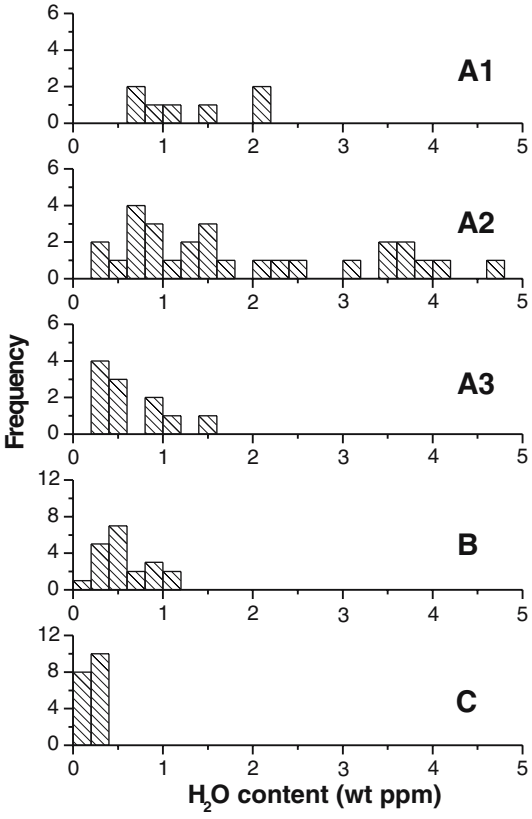

Fig. 5 Analytical H_2O contents for spodumene samples of different genetic types calculated on the basis of Lambert–Beer's law. Note the different frequency scales for different spodumene types

chemistry, crystal structural constraints and/or chemical composition, specifically the presence of minor-to-trace elements acting as a charge balance (Skogby et al. 1990; Andrut et al. 2003), were reported to control the total OH defect concentrations in NAMs and especially in pyroxenes. However, post-crystallization changes, including late exchange of hydrogen between crystals and fluids, may also play an important role (Ingrin et al. 1995; Skogby 1999; Andrut et al. 2003; Koch-Müller et al. 2004).

Kohlstedt and Mackwell (1999) and Bromiley et al. (2004) experimentally observed that at low pressure the OH solubility in anhydrous silicates increases with increasing water fugacity. Similarly, Arredondo et al. (2001) studied the hydrogen content in natural garnets from granitic pegmatites and found an increase with gradually increasing activity of H_2O during pegmatite crystallization, i.e., from the wall zone to the core zone (Arredondo et al. 2001). However, assuming an increase of activity of H_2O from magmatic to hydrothermal stage of pegmatite formation (cf. London 1986a; Lumpkin 1998), the elevated hydrogen contents in magmatic spodumene with respect to low hydrogen content in hydrothermal spodumene (cf. Fig. 5) follow an opposite trend. Unfortunately, the changes in activity of H_2O from magmatic to hydrothermal stage could not be quantified. Nevertheless, comparing Table 1 and Fig. 5, enhanced *P–T* conditions are apparently reflected by enhanced OH defect concentrations in the respective spodumene samples, where LT/LP hydrothermal spodumene clearly contains the lowest OH defect concentrations (Fig. 5). Taking into account that pegmatites originate from melts or fluids rich in hydrous components (cf. London 1986a) and with respect to the common presence of hydrous minerals (chiefly micas) associated with spodumene, the low hydrogen content and its differences within particular genetic types of spodumene likely do not reflect the activity of hydrous components during crystallization. Consequently, the OH defect concentrations in spodumene are likely related to maximum solubility of hydrogen in the spodumene structure at given *P–T* conditions and at actual chemical composition of spodumene.

Moreover, hydrothermal spodumene, rich in fluid inclusions (e.g., Sp10, Sp27a), reveals the lowest OH defect concentrations (cf. Table 3). Thus, spodumene most likely preserved its original hydrogen concentrations, and late exchange of hydrogen between crystals and fluid inclusions seem to be negligible. The determined hydrogen content is the result of a primary OH incorporation into the structure of spodumene and not of a late secondary alteration process.

The incorporation of hydrogen into the pyroxene structure may partly follow the reaction (Skogby and Rossman 1989), $Fe^{3+} + O^{2-} + 1/2H_2 = Fe^{2+} + OH^-$. However, there is generally no evident relationship of the OH defect concentrations on the Fe contents (compare Figs. 2, 5). Moreover, no apparent correlation between the OH defect concentration and the Fe^{2+} content calculated on the basis of Mössbauer spectroscopy exists (compare Table. 3, 5). With respect to the extremely low OH defects concentrations, their presence can be related to elements present in concentrations below the detection limit of EMPA or, according to our model of OH defect incorporation (see previous section), to the availability of M site vacancies.

Altogether, both chemical composition (i.e., low presence of vacancies) and low *P–T* conditions during the crystallization of spodumene very likely control the low extent of OH defect incorporation into its crystal structure. Considering the high OH defect concentrations of high *P–T* pyroxenes from upper mantle rocks (up to 1,200 wt ppm OH; Skogby 1999; Ingrin and Skogby 2000), the low OH defect concentrations in spodumene (< 5 wt ppm H_2O) follows very well the trend that LT/LP NAMs generally contain lower hydrogen contents compared to HT/HP ones (see Skogby 1999). These results are in agreement with petrologic models of the formation of granitic pegmatites at *P–T* conditions of the upper crust, where spodumene formation ranges at $P \sim 1$–$4(6)$ kbar and $T \sim 650$–400°C (Table 1). Regarding the extremely low hydrogen content in spodumene, insignificant changes of the univariant curves position within the *P–T* diagram (see London 1984; Krivovichev 2004) are indicated.

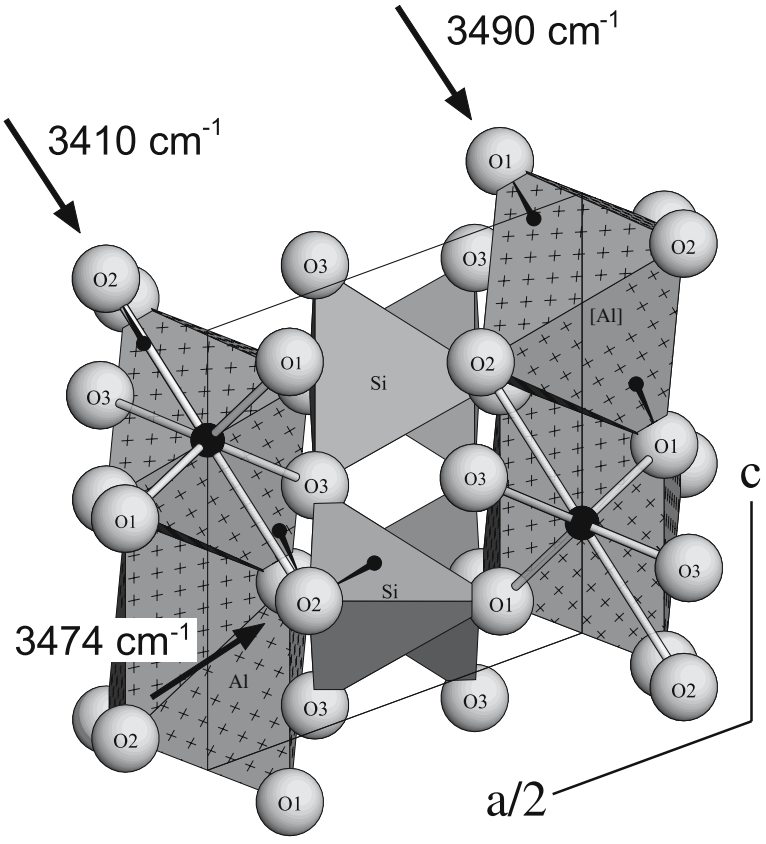

Fig. 6 Part of spodumene structure with suggested structural positions of hydrogen. Wavenumbers of corresponding FTIR absorption bands (or group of bands) are indicated (see text). *Large black circles* Li (or vacancy in case of hydrogen substitution); *small black circles* hydrogen

Acknowledgement This work has been supported by a Marie Curie Fellowship of the European Commission under contract number HPMT-CT-2000-00138 to JF and by research projects of Ministry of Education of Czech Republic (MSM0021622412 to MN and MSM6198959218 to RZ). Major part of this work has been done during stay of JF at the University of Vienna. We wish to thank A. Wagner for his delicate sample preparation, U. Kolitsch, A. Wieczorek, J. Leichmann, R. Škoda and M. Mashlan for technical assistance. Samples for this study were kindly provided by the Moravian Museum in Brno, Czech Republic, E. Libowitzky and M. Bohatý.

References

Andrut M, Brandstatter F, Beran A (2003) Trace hydrogen zoning in diopside. Miner Petrol 78:231–241

Arredondo EH, Rossman GR, Lumpkin GR (2001) Hydrogen in spessartine–almandine garnets as a tracer of granitic pegmatite evolution. Am Mineral 86:485–490

Bai Q, Kohlstedt DL (1993) Effects of chemical environment on the solubility and incorporation mechanism for hydrogen in olivine. Phys Chem Miner 19:460–471

Bell DR, Rossman GR (1992) Water in Earth's mantle: the role of nominally anhydrous minerals. Science 255:1391–1397

Bell DR, Ihinger PD, Rossman GR (1995) Quantitative analysis of trace OH in garnet and pyroxenes. Am Mineral 80:465–474

Bell DR, Rossman GR, Maldener J, Endisch D, Rauch F (2004) Hydroxide in kyanite: a quantitative determination of the absolute amount and calibration of the IR spectrum. Am Mineral 89:998–1003

Beran A (1999) Contribution of IR spectroscopy to the problem of water in the Earth's mantle. In: Wrigt K, Catlow R (eds) Microscopic properties and processes in minerals. Kluwer, Holland, pp 523–538

Beran A (2002) Infrared spectroscopy of micas. In: Mottana A et al (eds) Micas: crystal chemistry and metamorphic petrology. Rev Miner Geochem 46:351–369

Beran A, Libowitzky E (2003) IR spectroscopic characterization of OH defects in mineral phases. Phase Transit 76:1–15

Beran A, Langer K, Andrut M (1993) Single crystal infrared spectra in the range of OH fundamentals of paragenetic garnet, omphacite and kyanite in an eklogitic mantle xenolith. Miner Petrol 48:257–268

Bromiley GD, Keppler H, McCammon C, Bromiley FA, Jacobsen SD (2004) Hydrogen solubility and speciation in natural, gem-quality chromian diopside. Am Mineral 89:941–949

Černý P (1982a) Anatomy and classification of granitic pegmatites. In: Černý P (ed) Granitic pegmatites in science and industry. Short course handbook 8. Mineralogical Association of Canada, pp 1–39

Černý P (1982b) Petrogenesis of granitic pegmatites. In: Černý P (ed) Granitic pegmatites in science and industry. Short course handbook 8. Mineralogical Association of Canada, pp 405–461

Černý P (1991) Rare-element granitic pegmatites. I. Anatomy and internal evolution of pegmatite deposits. Geosci Can 18:49–67

Černý P (2004) The Tanco rare-element pegmatite deposit, Manitoba: regional context, internal anatomy, and global comparisons. In: Linnen RL, Samson IM (eds) Rare-element geochemistry and ore deposits. Short course handbook 17. Geological Association of Canada, pp 184–231

Černý P, Ercit TS (2005) Classification of granitic pegmatites. Can Mineral (in press)

Černý P, Trueman DL, Ziehlke DV, Goad BE, Paul BJ (1981) The Cat Lake–Winnipeg River and the Wekusko Lake pegmatite fields, Manitoba. Manitoba energy & mines. Econ Geol Rep ER80-1, pp 1–234

Chakoumakos BC, Lumpkin GR (1990) Pressure–temperature constraints on the crystallization of the Harding pegmatite, Taos County, New Mexico. Can Mineral 28:287–298

Charoy B, Lhote F, Dusausoy Y (1992) The crystal chemistry of spodumene in some granitic aplite-pegmatites of northern Portugal. Can Mineral 30:639–651

Charoy B, Noronha F, Lima A (2001) Spodumene–petalite–eucryptite: mutual relationships and pattern of alteration in Li-rich aplite-pegmatite dykes from northern Portugal. Can Mineral 39:729–746

Clark JR, Appleman DE, Papike JJ (1969) Crystal-chemical characterization of clinopyroxenes based on eight new structure refinements. Special paper 2. Mineralogical Society of America, pp 31–50

Deer WA, Howie RA, Zussman J (1997) Rock-forming minerals, 2nd edn. Single-chain silicates, vol 2A. Geological Society, London, pp 1–668

De Grave E, Eeckhout SG (2003) ^{57}Fe Mössbauer-effect studies of Ca-rich, Fe-bearing clinopyroxenes: Part III. Diopside. Am Mineral 88:1145–1152

Dollase WA, Gustafson WI (1982) ^{57}Fe Mössbauer spectral analysis of the sodic clinopyroxenes. Am Mineral 67:311–327

Doria A, Charoy B, Noronha F (1989) Fluid inclusion studies in spodumene-bearing aplite-pegmatite dykes of Covas de Barroso, Northern Portugal. In: ECROFI X, London, p 25

Farmer VC (1974) The infrared spectra of minerals. Monograph No. 4. Mineralogical Society, London, pp 1–539

Foord EE, Starkey HC, Taggert JE Jr (1986) Mineralogy and paragenesis of "pocket" clays and associated minerals in complex granitic pegmatites, San Diego County, California. Am Mineral 71:428–439

Foord EE, London D, Kampf AR, Shigley JE, Snee LW (1991) Gem-bearing pegmatites of San Diego County, California. In: Walamender MJ, Hanan BB (eds) Geological excursions in Southern California and Mexico. Field Trip Guidebook for the 1991 Annual Meeting. Geological Society America, San Diego, pp 128–146

Göd R (1989) The spodumene deposit at "Weinebene", Koralalpe, Austria. Miner Deposita 24:270–278

Graham J (1975) Some notes on α–spodumene, LiAlSi2O6. Am Mineral 60:919–923

Ingrin J, Skogby H (2000) Hydrogen in nominally anhydrous upper-mantle minerals: concentrations levels and implications. Eur J Mineral 12:543–570

Ingrin J, Hercule S, Charton T (1995) Diffusion of hydrogen in diopside—results of dehydration experiments. J Geophys Res 100(B8):15489–15499

Kazmi AH, Peters JJ, Obodda HP (1985) Gem pegmatites of the Shingus-Dusso Area, Gilgit, Pakistan. Mineral Rec 16:393–411

Keppler H, Rauch M (2000) Water solubility in nominally anhydrous minerals measured by FTIR and ^{1}H MAS NMR: the effect of sample preparation. Phys Chem Miner 27:371–376

Koch-Müller M, Matsyuk SS, Wirth R (2004) Hydroxyl in omphacites and omphacitic clinopyroxenes of upper mantle to lower crustal origin beneath the Siberian platform. Am Mineral 89:921–931

Kohlstedt DL, Mackwell SJ (1999) Solubility and diffusion of "water" in silicate minerals. In: Wrigt K, Catlow R (eds) Microscopic properties and processes in minerals. Kluwer, Holland, pp 539–559

Krivovichev VG (2004) Mineral equilibria with spodumene, petalite and eucryptite. I. System Li_2O–Al_2O_3–SiO_2–H_2O—thermodynamical analysis and geological application. Proc Russ Mineral Soc 133:1

Kunasz I (1982) Foote Mineral Company—Kings mountain operation. In: Černý P (ed) Granitic pegmatites in science and industry. Short course handbook 8. Mineralogical Association of Canada, pp 505–511

Libowitzky E (1999) Correlation of O–H stretching frequencies and O–H···O hydrogen bond lengths in minerals. Monatsh Chem 130:1047–1059

Libowitzky E, Beran A (2004) IR spectroscopic characterization of hydrous species in minerals. In: Beran A, Libowitzky E (eds) EMU notes in mineralogy 6. Eötvös Univ Press, Budapest, pp 227–279

Libowitzky E, Rossman GR (1996) Principles of quantitative absorbance measurements in anisotropic crystals. Phys Chem Miner 23:319–327

Libowitzky E, Rossman GR (1997) An IR absorption calibration for water in minerals. Am Mineral 82:1111–1115

London D (1984) Experimental phase equilibria in the system $LiAlSiO_4$–SiO_2–H_2O: a petrogenetic grid for lithium-rich pegmatites. Am Mineral 69:995–1004

London D (1986a) Magmatic-hydrothermal transition in the Tanco rare-element pegmatite: evidence from fluid inclusions and phase equilibrium experiments. Am Mineral 71:376–395

London D (1986b) Formation of tourmaline-rich gem pockets in miarolitic pegmatites. Am Mineral 71:396–405

London D (2004) Geochemistry of alkali and alkaline earth elements in ore-forming granites, pegmatites and rhyolites. In: Linnen RL, Samson IM (eds) Rare-element geochemistry and ore deposits. Short course notes 17, Geological Association of Canada, pp 25–69

London D, Burt DM (1982) Lithium minerals in pegmatites. In: Černý P (ed) Granitic pegmatites in science and industry. Short course handbook 8. Mineralogical Association of Canada, pp 99–133

Losos Z, Beran A (2004) OH defects in cassiterite. Miner Petrol 81:219–234

Lumpkin GR (1998) Rare-element mineralogy and internal evolution of the Rutherford no. 2 pegmatite, Amelia County, Virginia: a classic locality revisited. Can Mineral 36:339–353

Makrygina VA, Makagon VM, Zagorsky VE, Shmakin BM (1990) Mica-bearing pegmatites (in Russian). Nauka, Siberia, pp 1–233

Merlet C (1994) An accurate computer correction program for quantitative electron probe microanalysis. Mikrochim Acta 114/115:363–376

Mulja T, Williams-Jones AE, Wood SA, Boily M (1995) The rare-element-enriched monzogranite–pegmatite–quartz vein systems in the Preissac–Lacorne batholith, Quebec. II. Geochemistry and petrogenesis. Can Mineral 33:817–822

Paterson MS (1982) The determination of hydroxyl by infrared absorption in quartz, silicate glasses and similar materials. Bull Mineral 105:20–29

Rossman GR (1996) Studies of OH in nominally anhydrous minerals. Phys Chem Miner 23:299–304

Skogby H (1999) Water in nominally anhydrous minerals. In: Wright K, Catlow R (eds) Microscopic properties and processes in minerals. Kluwer, Holland, pp 509–522

Skogby H, Rossman GR (1989) OH^- in pyroxene: an experimental study of incorporation mechanisms and stability. Am Mineral 74:1059–1069

Skogby H, Bell DR, Rossman GR (1990) Hydroxide in pyroxene: variations in the natural environment. Am Mineral 75:764–774

Smeds SA, Černý P (1989) Pollucite from the Proterozoic petalite-bearing pegmatites of Uto, Stockholm archipelago, Sweden. Geol Förenin Stockholm Förh 111:361–372

Spear FS (1993) Metamorphic phase equilibria and pressure–temperature–time paths. Mineralogical Society of America Monograph, Washington, pp 1–799

Stalder R (2004) Influence of Fe, Cr and Al on hydrogen incorporation in orthopyroxene. Eur J Mineral 16:703–711

Taylor BE, Foord EE, Friedrichsen B (1979) Stable isotope and fluid-inclusion studies of gem-bearing granitic pegmatite-aplite dikes, San Diego Co., California. Contrib Mineral Petrol 68:187–205

Thomas AV, Pasteris JD, Bray CJ, Spooner ETC (1990) H_2O–CH_4–NaCl–CO_2 inclusions from the footwall contact of the Tanco granitic pegmatite: estimates of internal pressure and

composition from microthermometry, laser Raman spectroscopy, and gas chromatography. Geochim Cosmochim Acta 54:539–573

Veblen DR, Buseck PR (1981) Hydrous pyriboles and sheet silicates in pyroxenes and uralites: intergrown microstructures and reaction mechanisms. Am Mineral 66:1107–1134

Walker RJ, Hanson GN, Papike JJ, ÓNeil JR, Laul JC (1986) Internal evolution of the Tin Mountain pegmatite, Black Hills, South Dakota. Am Mineral 71:440–459